

Mn₇ Species with an $S = 29/2$ Ground State: High-Frequency EPR Studies of a Species at the Classical/Quantum Spin Interface

Zhenxing Wang,[†] Johan van Tol,^{*,†} Taketo Taguchi,[‡] Matthew R. Daniels,[‡] George Christou,[‡] and Naresh S. Dalal^{*,†}

[†]Department of Chemistry and Biochemistry, and National High Magnetic Field Laboratory, Florida State University, Tallahassee, Florida 32306, United States

[‡]Department of Chemistry, University of Florida, Gainesville, Florida 32611-7200, United States

S Supporting Information

ABSTRACT: A high spin (S) compound has been synthesized whose properties straddle the interface between the classical and quantum mechanical spin descriptions. The cluster $[\text{Mn}_7\text{O}_4(\text{pdpm})_6(\text{N}_3)_4](\text{ClO}_4)_2$ (**Mn₇**) has an unprecedented core structure comprising an octahedral $[\text{Mn}^{\text{III}}_6(\mu_4\text{-O})(\mu_3\text{-O})_3(\mu_3\text{-N}_3)_4]^{6+}$ unit with one of its faces capped by a Mn^{II} ion. Magnetization and susceptibility studies indicate an $S = 29/2$ ground state, the maximum possible. Variable-temperature, high-frequency electron paramagnetic resonance (HF-EPR) spectra on powder and single-crystal samples of **Mn₇** exhibit sharp spectral features characteristic of a quantum spin that are well resolved in a certain temperature range but which transform to a continuum of peaks characteristic of a classical spin in another; these features have been well reproduced by computer simulations. A fast Fourier transform analysis of the sharp spectral features and the low temperature EPR spectra suggests that more than one spin state are involved.

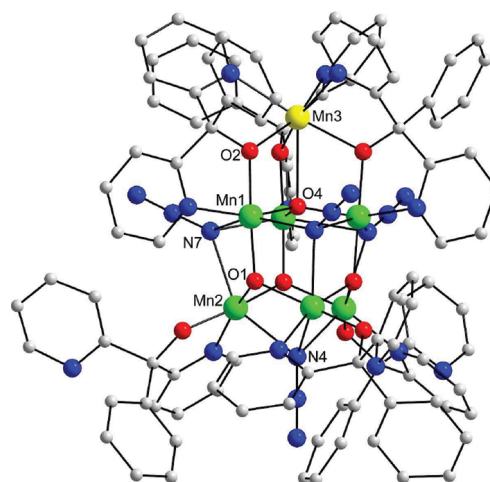


Figure 1. The structure of the **Mn₇** cation. The C_3 -axis is vertical, passing through Mn3, O4, and N4. H atoms have been omitted for clarity. Color code: Mn^{II} , yellow; Mn^{III} , green; O, red; N, blue; C, gray.

The discovery of single molecule magnets (SMMs),¹ in which each molecule behaves as a magnetic domain,² has opened a fertile area for developing molecular electronics as well as for a fundamentally new way of understanding the quantum chemistry and physics of the electron spin.³ It was noted early on that a prerequisite for SMM behavior was the existence of a large barrier to spin reversal whose upper limit is given by DS^2 , where D is the zero-field uniaxial anisotropy parameter and S is the total spin. Thus, in general, a large spin S in combination with a large negative anisotropy parameter D is required for possible SMM applications, e.g., in quantum computing.^{2–4}

For the above reasons, we and others have been developing new synthetic methods for Mn clusters of various sizes and, to date, have successfully isolated and studied a wide variety, with nuclearities up to 84.⁵ While these compounds have provided a plethora of new structural, magnetic, and spectroscopic data, it was noted that the spin dynamics exhibited by clusters with particularly large values of S showed spectroscopic features that could not be well simulated using a quantum mechanical description of the spin S . A clear example of this is that the electron paramagnetic resonance (EPR) spectra of many of these compounds^{6–8} were found to yield spectra that exhibited a continuum rather than the series of well resolved peaks that have been the hallmark of compounds with $S = 10$ or smaller.⁹

These observations suggested that there might be a spin-phase classical-quantum boundary, and we have been searching for compounds at this boundary among the various Mn clusters that we have been synthesizing and studying in recent years, concentrating on moderate size clusters with large spin S . Here, we report the magnetic and EPR characterization of a new cluster $[\text{Mn}_7\text{O}_4(\text{pdpm})_6(\text{N}_3)_4](\text{ClO}_4)_2$ (**Mn₇**). It has an unprecedented core structure, but more significant is the discovery that the properties of this cluster with an $S = 29/2$ ground state place it at the classical/quantum spin interface.

Mn₇ was prepared from the 1:1:1:1 reaction of $\text{Mn}(\text{ClO}_4)_2$, NaN_3 , NEt_3 , and phenyl(dipyridin-2-yl)methanol (pdpmH) in MeCN/MeOH (20:1 v/v) and isolated in ~50% yield as dark red crystals of **Mn₇**·2MeCN on layering of the filtered solution with Et_2O . The **Mn₇** cation (Figure 1) has C_3 symmetry, and its core consists of a $[\text{Mn}^{\text{III}}_6(\mu_4\text{-O})(\mu_3\text{-O})_3(\mu_3\text{-N}_3)_4]^{6+}$ unit, with one of its faces capped by a Mn^{II} atom. Three η^2 -chelating and three η^2 : μ -chelating/bridging pdpm[−] groups provide the peripheral ligation.

Variable-temperature magnetic susceptibility measurements were performed on a microcrystalline powder sample, restrained

Received: August 12, 2011

Published: October 09, 2011

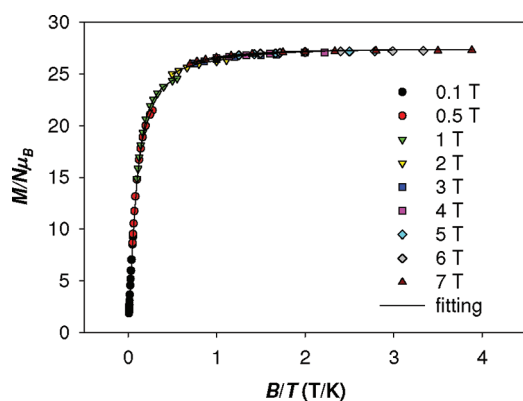


Figure 2. Plots of reduced magnetization ($M/N\mu_B$) vs B/T . The solid lines are the fit of the data; see the text for the fit parameters.

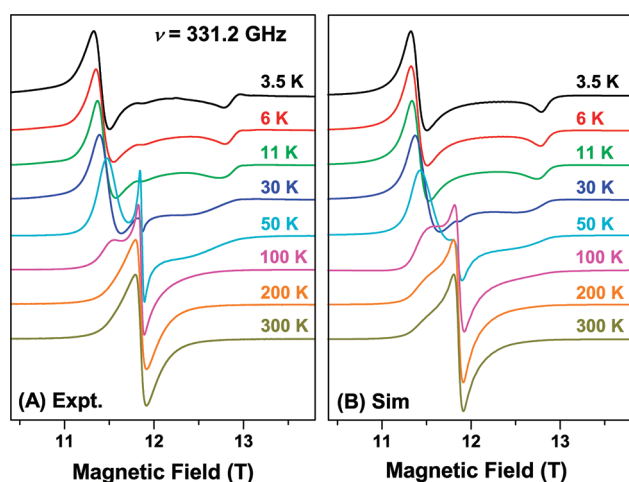


Figure 3. EPR spectra of a powder sample at 331.2 GHz as a function of temperature. (A) Experimental; (B) simulation (see text). The amplitudes of the spectra are normalized.

in eicosane, in a 0.1 T field and in the 5.0–300 K range. The $\chi_M T$ gradually increases from $30.59 \text{ cm}^3 \cdot \text{K} \cdot \text{mol}^{-1}$ at 300 K to a value of $102.81 \text{ cm}^3 \cdot \text{K} \cdot \text{mol}^{-1}$ at 8 K, and then slightly decreases to 102.09 at 5.0 K. The plot profile indicates dominant ferromagnetic interactions, and the 5.0 K value suggests an $S_T = {}^{29}/_2$ ground state with $g \sim 1.91$; the spin-only value is $112.38 \text{ cm}^3 \cdot \text{K} \cdot \text{mol}^{-1}$. $S_T = {}^{29}/_2$ is the maximum possible for Mn_7 , indicating a completely ferromagnetically coupled system.

In order to confirm the ground state and determine the zero-field splitting parameter D , magnetization vs applied field data were collected on a restrained sample in the 0.1–7 T and 1.8–10.0 K ranges. The resulting data were fit, using the program MAGNET,¹⁰ by diagonalization of the spin Hamiltonian matrix assuming that only the ground state is populated, incorporating axial anisotropy ($D\hat{S}_z^2$) and Zeeman terms, and employing a full powder average.

The resulting data are shown in Figure 2 as reduced magnetization ($M/N\mu_B$) vs B/T , where N is Avogadro's number. The isofield lines are essentially superimposed, indicating minimal anisotropy (D -value). The fit (solid lines in Figure 2) was obtained with $S_T = {}^{29}/_2$, $g = 1.89(2)$, and $D = 0.03(1) \text{ cm}^{-1}$. An equally good fit was obtained with $S_T = {}^{29}/_2$, $g = 1.89(1)$, and $D = -0.020(5) \text{ cm}^{-1}$. It is

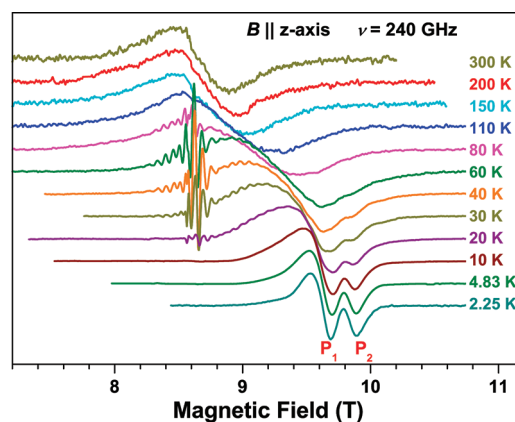


Figure 4. EPR spectra of a single crystal at 240 GHz with the field parallel to the z -axis. The amplitudes are normalized.

common to obtain two acceptable fits of magnetization data for a given spin S , with $D > 0$ and $D < 0$, because magnetization fits are not very sensitive to the sign of D . The unusually low g -value is undoubtedly an artifact reflecting the presence of a very low-lying excited state populated even at these low temperatures (vide infra) and the generally low reliability of g -values from powder susceptibility fits; for Mn^{III} -containing complexes, a g -value only slightly less than 2 is expected and usually observed.

For an independent assessment of the ground state S , the g -value and the sign and magnitude of the axial Zero-Field Splitting (ZFS) parameter D , EPR measurements^{11,12} were carried out on Mn_7 in the solid state. Figure 3A shows the temperature dependence of the EPR spectrum of the powder sample at 331.2 GHz. The spectrum is a broad peak at 300 K, but new features start to develop at lower temperatures. At the lowest temperature, the spectrum resembles a typical powder pattern for axial symmetry. The transitions for the field along the principal axis of the ZFS tensor appear on the high field side (Figure S1, Supporting Information), which indicates that D is positive. In cases like this with a very large ground spin state, the $2S$ EPR fine-structure peaks are not resolved when the magnitude of D is smaller than the line-width, and it is only possible to estimate the product DS .^{6,7} However, the g -value can be determined with a good precision. To simulate the powder EPR spectra, we utilized the following Hamiltonian

$$\hat{H} = g\mu_B \mathbf{B} \cdot \hat{\mathbf{S}} + D(\hat{S}_z^2 - \hat{S}^2/3) + E(\hat{S}_x^2 - \hat{S}_y^2) \quad (1)$$

in which we now also include the strain parameters ΔD and ΔE , which are the full width at half maximum (fwhm) of a Lorentzian distribution around average D and E values due to the spread of the local crystal-field distortions of the molecules.¹³ Because of the 3-fold symmetry, we have kept $E = 0$ but allow ΔE to vary.

The simulation in Figure 3B was obtained with the following spin Hamiltonian parameters: $S = {}^{29}/_2$, $g = 1.996(1)$, $D = 0.0320(2) \text{ cm}^{-1}$, $\Delta D = 0.010(2) \text{ cm}^{-1}$, $E = 0$, $\Delta E = 0.008(2) \text{ cm}^{-1}$.¹⁴ Although this simulation assumes that only the $S = {}^{29}/_2$ spin state is populated over the whole temperature range, it can be seen that the overall change of spectra with temperature is well simulated, and the simulation confirms a positive sign of D and gives a much more accurate g -value than can be deduced from susceptibility fits. The sharp peaks in the center of the spectra correspond to the $\Delta m_S = \pm 1$ transitions involving spin sublevels with small quantum numbers $m_S = \pm 1/2, \pm 3/2, \pm 5/2$,

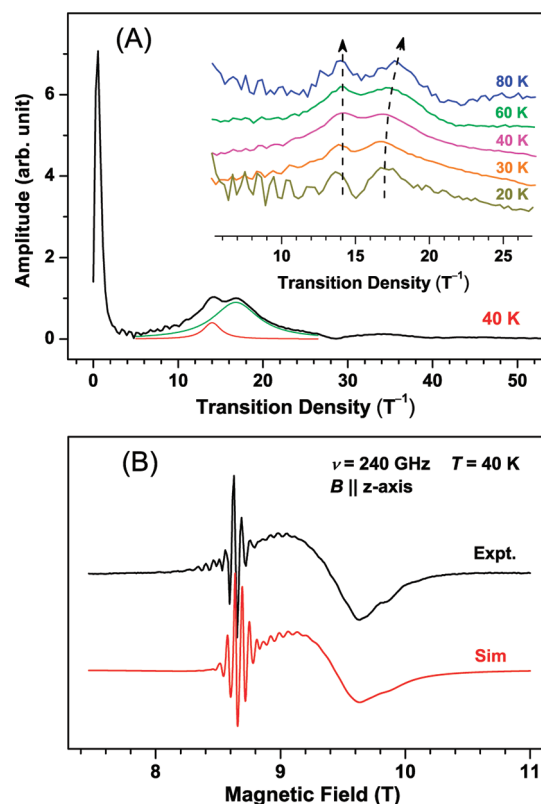


Figure 5. (A) FFT of the 40 K EPR spectrum in Figure 4 and its fitting with two Gaussian peaks. Inset: FFT of the EPR spectra at different temperatures. (B) EPR spectrum of a single crystal at 40 K with the field parallel to the *z*-axis, and its simulation.

etc, which have higher transition probability and are less broadened by *D* and *E* strain. These spectra are a perfect experimental realization of the theoretical spectral simulations by Fittipaldi¹⁵ et al. for a similarly large spin system, but with a different sign of the ZFS parameter *D*.

The central peak in the experimental spectra observed at higher temperatures is slightly stronger than in the simulations. Also, the simulated spectra above 200 K display more of a low field shoulder than the experiments. We suspect that these observations are due to the deviation from a simple model that assumes only a single well-defined $S_T = ^{29}/_2$ spin state is populated. To clarify this, measurements were made using single crystals. The orientational dependence of the 8 K spectra are shown in Figure S2 (Supporting Information), whereas Figure 4 shows 240 GHz spectra at various temperatures with the magnetic field aligned along the main axis of the axial zero-field splitting tensor (*z*-axis). At 300 K, the spectra from the single crystal also yielded a single Lorentzian peak, but as the temperature is lowered, the peak broadens, shifts to higher field, and fine-structure peaks start to develop below 110 K. These fine structure peaks disappear below 20 K. The magnitude of the splitting (~ 600 G) is too large to arise from hyperfine coupling¹⁶ and must be due to the ZFS of the Mn_7 complex.

At low temperatures, a second broad peak (P_2) appears and becomes stronger as the temperature decreases. It is seen that P_1 is not symmetric, and it is much broader and more intense than P_2 . This suggests that not only the ground spin state is populated, but excited states are involved in the observed EPR transitions.

These observations are not unreasonable if some exchange coupling constants in the molecule are not too large compared to kT . We also observed similar phenomena in the HF-EPR study on Mn_{25} , with $S = ^{61}/_2$.⁸

In order to confirm the assumption of at least two spin states contributing to the observed signals, we employed a relatively unusual procedure for analyzing the fine structure of such a high spin system. Figure 5A shows a fast Fourier transform (FFT) of the single-crystal EPR spectrum at 40 K. The units (T^{-1}) of the horizontal axis correspond to the number of oscillations per Tesla of magnetic field, which we call the “transition density” n_T . The peak at $\sim 0.5 T^{-1}$ is assigned to the broad background that dominates the EPR spectrum (Figure 4). Two peaks were observed at around $15 T^{-1}$, which are related to the fine structure in the cw spectrum at around 8.6 T ($g \approx 1.996$). The Fourier transform shows that two oscillation frequencies can clearly be distinguished, which correspond to the spacing between two neighboring $m_S \rightarrow m_S + 1$ EPR transitions that should be equal to $2D$ for this orientation. Thus, we observe two different *D*-values that are presumably from two spin states. The two oscillation frequencies (14.1 and $16.9 T^{-1}$ at 20 K) appear to be slightly temperature-dependent (inset of Figure 5A), which might be due to the contribution of more spin states at higher temperatures. The corresponding *D*-values are 0.0329 and 0.0274 cm^{-1} , if we assume only second-order terms in the ZFS ($2D = g\mu_B/n_T$). Over the temperature range of 20–80 K, the relative amplitude of the two peaks remains similar, indicating that the energy difference between the two spin states is small. However, in the low temperature spectra, the position of P_1 and P_2 for $S = ^{27}/_2$ or $S = ^{29}/_2$ corresponds to a slightly larger value of *D*. To account for this discrepancy, we have introduced an additional fourth order term in the Hamiltonian:

$$\hat{H} = g\mu_B \mathbf{B} \cdot \hat{\mathbf{S}} + D(\hat{S}_z^2 - \hat{S}^2/3) + B_4^0 \hat{O}_4^0 \quad (2)$$

where \hat{O}_4^0 is the standard Stevens’ operator.¹⁶ As we are only considering the spectrum for $B||z$ -axis, we do not include the nonaxial second order term ($E = 0, \Delta E = 0$).

Figure 5B shows the simulation to the spectrum at 40 K assuming two spin states, an $S = ^{29}/_2$ ground state and an $S = ^{27}/_2$ first excited state. The resulting parameters are (a) ground state, $S = ^{29}/_2, g = 1.996, D = 0.035 \text{ cm}^{-1}, \Delta D = 0.007(2) \text{ cm}^{-1}, B_4^0 = 5.7(2) \times 10^{-7} \text{ cm}^{-1}$; and (b) first excited state, $S = ^{27}/_2, g = 1.996, D = 0.030 \text{ cm}^{-1}, \Delta D = 0.009(2) \text{ cm}^{-1}, B_4^0 = 7.5(2) \times 10^{-7} \text{ cm}^{-1}$. The intrinsic line width (without *D*- and *E*-strain) is about 35 mT, which is likely due to dipolar coupling with surrounding molecules. The values found for the fourth order term appear reasonable, as the ratio of D/B_4^0 is similar to that found in systems like Mn_{12} ¹⁷ and Fe_8 .¹⁸ The same parameters also provide a reasonable simulation of the 2.25 K spectrum, as shown in Figure S3 (Supporting Information). It thus is possible to describe the low temperature (<80 K) EPR spectra on the basis of a population of two closely spaced spin states. Although the magnetization data in Figure 2 were fitted on the basis of a single $S = ^{29}/_2$ state, the obtained *g*-value of 1.89 is 5.5% lower than the value determined experimentally by EPR. Using the experimentally determined *g*-value, the saturation magnetization agrees well with a mixture of $S = ^{29}/_2$ and $S = ^{27}/_2$ spin states. Of course, from our analysis it cannot be excluded that additional spin states are populated, especially at higher temperatures. This might explain the disappearance of the structures above 80 K, but line broadening due to increased relaxation at higher temperatures can

also play a role. The shift of the higher frequency component in the Fourier transforms (inset of Figure 5A) at higher temperatures might indicate that more spin states with smaller D -values are populated above 40 K. This new FFT-analysis procedure could prove to be useful in the detailed analysis of the EPR spectra of such high spin multiplets.

In conclusion, the Mn_7 complex with an $S = 29/2$ ground state was investigated in detail by HF-EPR spectroscopy and magnetic susceptibility, as this system was considered attractive for examining the transition from quantum to classical behavior of a large spin system. We indeed found that the compound yielded spectra that exhibit both broad unresolved features but also a fine structure that is well resolved in a limited temperature range. In other words, it exhibits the spectral signatures of both classical and quantum spins. Thus, this Mn_7 cluster provides the first clear experimental realization of the simulated spectral predictions for such a large spin system. In addition, the temperature dependence of the powder spectrum illustrates changes in the spectrum that could be explained solely on the basis of D -strain and a redistribution of the population over the spin sublevels of a single spin state, spin levels that for a $S = 29/2$ system at 12 T span an energy range corresponding to 476 K. However, single crystal measurements resolved some of the transitions and showed that at least two spin states are involved. A FFT analysis was introduced as a powerful new procedure to analyze the newly observed splittings in the EPR spectra and to separate transitions from different spin states. This analysis confirmed the two peak structure that is observed in the low temperature spectra and gave an estimate for the fourth-order term in the Hamiltonian. Note that Mn_7 appears to possess an excellent combination of small metal nuclearity and large value of the total spin S to facilitate the above studies and allow the spectra to be reasonably explained, in this case, on the basis of two well-defined spin states. However, for larger systems such as the Mn_{84} cluster,^{5f} such a description becomes more problematic as many spin states are populated and transitions remain unresolved at all temperatures.

■ ASSOCIATED CONTENT

S Supporting Information. Supporting Figures S1–S3. This material is available free of charge via the Internet at <http://pubs.acs.org>.

■ AUTHOR INFORMATION

Corresponding Author

vantol@magnet.fsu.edu; dalal@chem.fsu.edu

■ ACKNOWLEDGMENT

We thank the National Science Foundation (CHE-0910472) for support of this work. The National High Magnetic Field Laboratory is supported by NSF Cooperative Agreement No. DMR-0654118 and by the State of Florida.

■ REFERENCES

- (1) (a) Sessoli, R.; Tsai, H. L.; Schake, A. R.; Wang, S.; Vincent, J. B.; Folting, K.; Gatteschi, D.; Christou, G.; Hendrickson, D. N. *J. Am. Chem. Soc.* **1993**, *115*, 1804. (b) Sessoli, R.; Gatteschi, D.; Caneschi, A.; Novak, M. A. *Nature* **1993**, *365*, 141. (c) Gatteschi, D.; Sessoli, R.; Villain, J. *Molecular Nanomagnets*; Oxford University Press: New York, 2006.
- (2) Christou, G.; Gatteschi, D.; Hendrickson, D. N.; Sessoli, R. *MRS Bull.* **2000**, *25*, 66.

- (3) Gatteschi, D.; Sessoli, R. *Angew. Chem., Int. Ed.* **2003**, *42*, 268.
- (4) Leuenberger, M. N.; Loss, D. *Nature* **2001**, *410*, 789.
- (5) Representative references are: (a) Aromi, G.; Brechin, E. K. *Struct. Bonding (Berlin, Ger.)* **2006**, *122*, 1. (b) Stamatatos, T. C.; Foguet-Albiol, D.; Stoumpos, C. C.; Raptopoulou, C. P.; Terzis, A.; Wernsdorfer, W.; Perlepes, S. P.; Christou, G. *J. Am. Chem. Soc.* **2005**, *127*, 15380. (c) Miyasaka, H.; Clérac, R.; Wernsdorfer, W.; Lecren, L.; Bonhomme, C.; Sugjura, K.; Yamashita, M. *Angew. Chem., Int. Ed.* **2004**, *43*, 2801. (d) Miliou, C. J.; Vinslava, A.; Wernsdorfer, W.; Moggach, S.; Parsons, S.; Perlepes, S. P.; Christou, G.; Brechin, E. K. *J. Am. Chem. Soc.* **2007**, *129*, 2754. (e) Miliou, C. J.; Raptopoulou, C. P.; Terzis, A.; Lloret, F.; Vicente, R.; Perlepes, S. P.; Escuer, A. *Angew. Chem., Int. Ed.* **2003**, *43*, 210. (f) Tasiopoulos, A. J.; Vinslava, A.; Wernsdorfer, W.; Abboud, K. A.; Christou, G. *Angew. Chem., Int. Ed.* **2004**, *43*, 2117. (g) Maheswaran, S.; Chastanet, G.; Teat, S. J. M. T.; Sessoli, R.; Wernsdorfer, W.; Winpenny, R. E. P. *Angew. Chem., Int. Ed.* **2005**, *44*, 5044. (h) Ako, A. M.; Hewitt, I. J.; Mereacre, V.; Clérac, R.; Wernsdorfer, W.; Anson, C. E.; Powell, A. K. *Angew. Chem., Int. Ed.* **2006**, *45*, 4926. (i) Aliaga-Alcalde, N.; Edwards, R. S.; Hill, S. O.; Wernsdorfer, W.; Folting, K.; Christou, G. *J. Am. Chem. Soc.* **2004**, *126*, 12503. (j) Brechin, E. K. *Chem. Commun.* **2005**, 5141. (k) Rajaraman, G.; Murugesu, M.; Soler, M.; Wernsdorfer, W.; Helliwell, M.; Teat, S. J.; Christou, G.; Brechin, E. K. *J. Am. Chem. Soc.* **2004**, *126*, 15445. (l) Murugesu, M.; Wernsdorfer, W.; Abboud, K. A.; Christou, G. *Angew. Chem., Int. Ed.* **2005**, *44*, 892. (m) Moushi, E. E.; Lampropoulos, C.; Wernsdorfer, W.; Nastopoulos, V.; Christou, G.; Tasiopoulos, A. J. *J. Am. Chem. Soc.* **2010**, *132*, 16146. (n) Zaleski, C. M.; Depperman, E. C.; Dendrinou-Samara, C.; Alexiou, M.; Kampf, J. W.; Kessissoglou, D. P.; Kirk, M. L.; Pecoraro, V. L. *J. Am. Chem. Soc.* **2005**, *127*, 12862. (o) Papaefstathiou, G. S.; Perlepes, S. P.; Escuer, A.; Vicente, R.; Font-Bardia, M.; Solans, X. *Angew. Chem., Int. Ed.* **2001**, *40*, 884.
- (6) Waldmann, O.; Ako, A. M.; Güdel, H. U.; Powell, A. K. *Inorg. Chem.* **2008**, *47*, 3486.
- (7) Murugesu, M.; Takahashi, S.; Wilson, A.; Abboud, K. A.; Wernsdorfer, W.; Hill, S.; Christou, G. *Inorg. Chem.* **2008**, *47*, 9459.
- (8) Wang, Z.; Stamatatos, T. C.; van Tol, J.; Nellutla, S.; Kaur, N.; Christou, G.; Dalal, N. S. unpublished.
- (9) (a) Hill, S.; Perenboom, J. A. A. J.; Dalal, N. S.; Hathaway, T.; Stalcup, T.; Brooks, J. S. *Phys. Rev. Lett.* **1998**, *80*, 2453. (b) Hill, S.; Maccagnano, S.; Park, K.; Achey, R. M.; North, J. M.; Dalal, N. S. *Phys. Rev. B: Condens. Matter Mater. Phys.* **2002**, *65*, 224410. (c) Hill, S.; Edwards, R. S.; Aliaga-Alcalde, N.; Christou, G. *Science* **2003**, *302*, 1015. (d) Wernsdorfer, W.; Aliaga-Alcalde, N.; Hendrickson, D. N.; Christou, G. *Nature* **2002**, *416*, 406.
- (10) Davidson, E. R. *MAGNET*; Indiana University: Bloomington, IN, 1999.
- (11) Morley, G. W.; Brunel, L. C.; van Tol, J. *Rev. Sci. Instrum.* **2008**, *79*, 064703.
- (12) van Tol, J.; Brunel, L. C.; Wyld, R. J. *Rev. Sci. Instrum.* **2005**, *76*, 074101.
- (13) Park, K.; Novotny, M. A.; Dalal, N. S.; Hill, S.; Rikvold, P. A. *Phys. Rev. B: Condens. Matter Mater. Phys.* **2001**, *65*, 014426.
- (14) Calculations were performed using EPRCalc developed by J.v.T.
- (15) Fittipaldi, M.; Sorace, L.; Barra, A. L.; Sangregorio, C.; Sessoli, R.; Gatteschi, D. *Phys. Chem. Chem. Phys.* **2009**, *11*, 6555.
- (16) Abragam, A.; Bleaney, B. *Electron Paramagnetic Resonance of Transition Ions*; Dover Publications: New York, 1986.
- (17) Hill, S.; Anderson, N.; Wilson, A.; Takahashi, S.; Chakov, N. E.; Murugesu, M.; North, J. M.; Dalal, N. S.; Christou, G. *J. Appl. Phys.* **2005**, *97*, 10M510.
- (18) Barra, A. L.; Gatteschi, D.; Sessoli, R. *Chem.—Eur. J.* **2000**, *6*, 1608.

SUPPORTING INFORMATION

Mn₇ Species with an $S = 29/2$ Ground State: High-Frequency EPR Studies of a Species at the Classical/Quantum Spin Interface

Zhenxing Wang,[‡] Johan van Tol,^{‡,*} Taketo Taguchi,[§] Matthew R. Daniels,[§] George Christou,[§] and Naresh S. Dalal,^{‡,*}

[‡] Department of Chemistry and Biochemistry, and National High Magnetic Field Laboratory, Florida State University, Tallahassee, Florida 32306, United States.

[§]Department of Chemistry, University of Florida, Gainesville, Florida 32611-7200, United States.

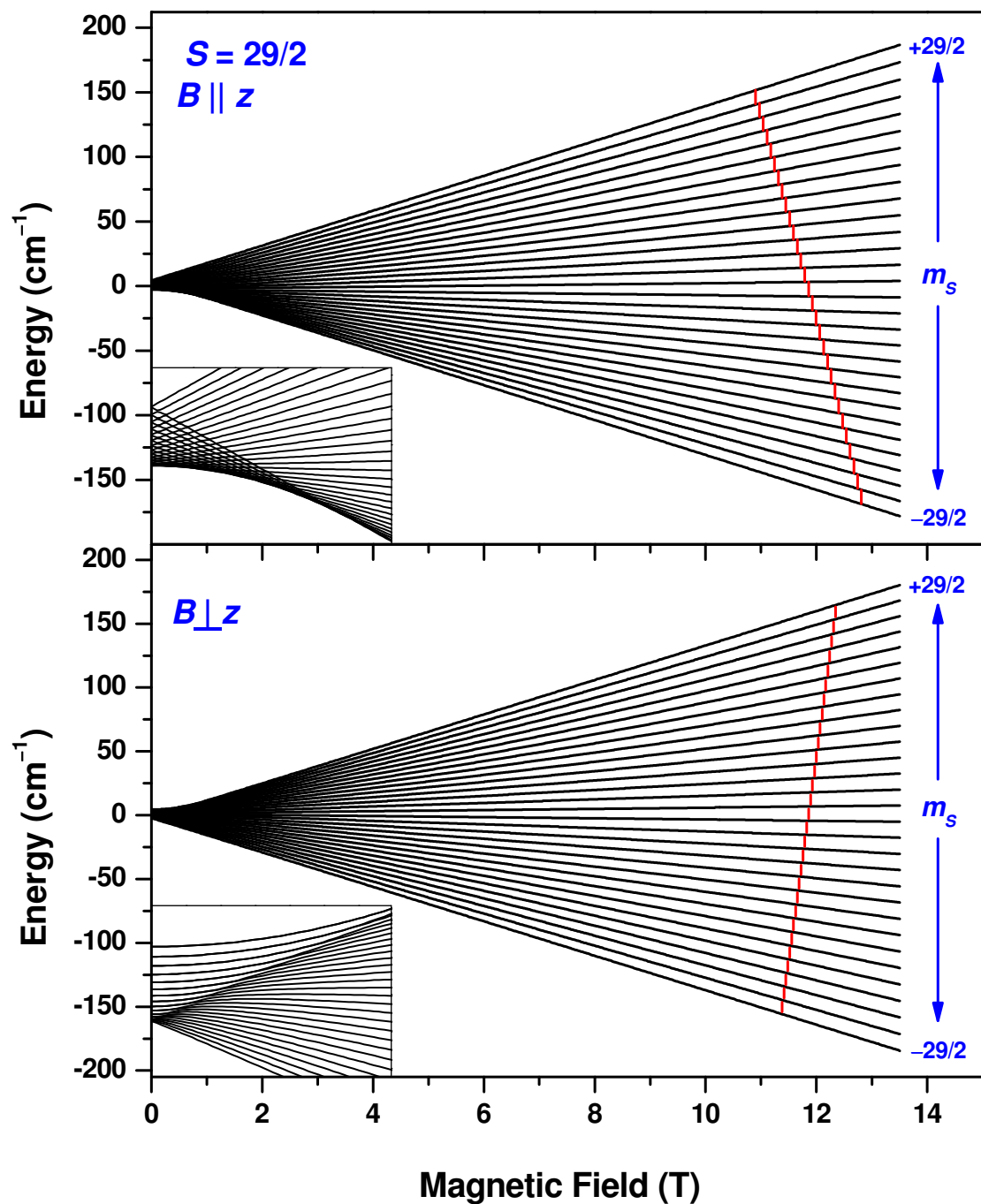


Figure S1. Zeeman energy levels of an $S = 29/2$ system with the ZFS parameter $D = +0.32 \text{ cm}^{-1}$ and $E = 0$. Upper panel: $B \parallel z$ -axis of the ZFS tensor. Bottom panel: $B \perp z$. The red lines indicate the allowed $\Delta m_s = \pm 1$ EPR transitions at 331.2 GHz. Insets: Low-field energy levels details. Note that at 12 T the spin sublevels cover a range of 300 cm^{-1} or 430 K. At the lowest temperatures only the lowest levels are occupied, resulting in the typical powder spectrum obtained at low temperature (Figure 3). For a negative D value the order of the levels would be inverted.

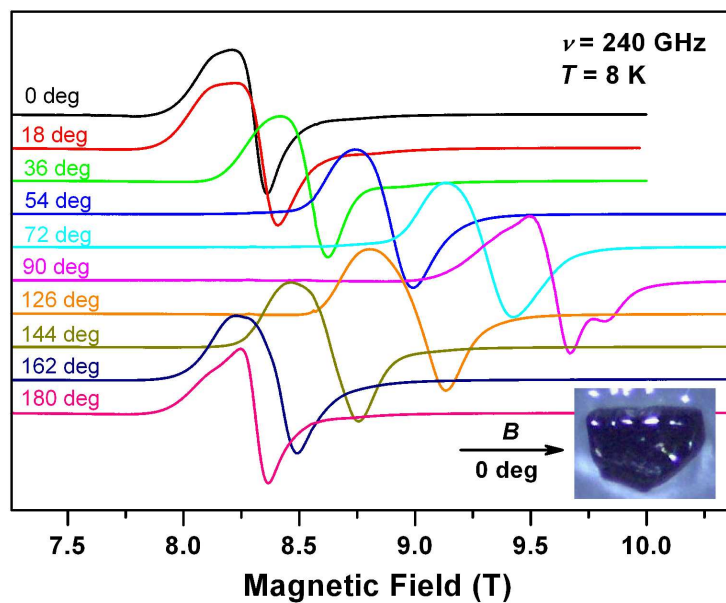


Figure S2. Angular dependence of the EPR spectra of a single crystal at 240 GHz and 8 K.

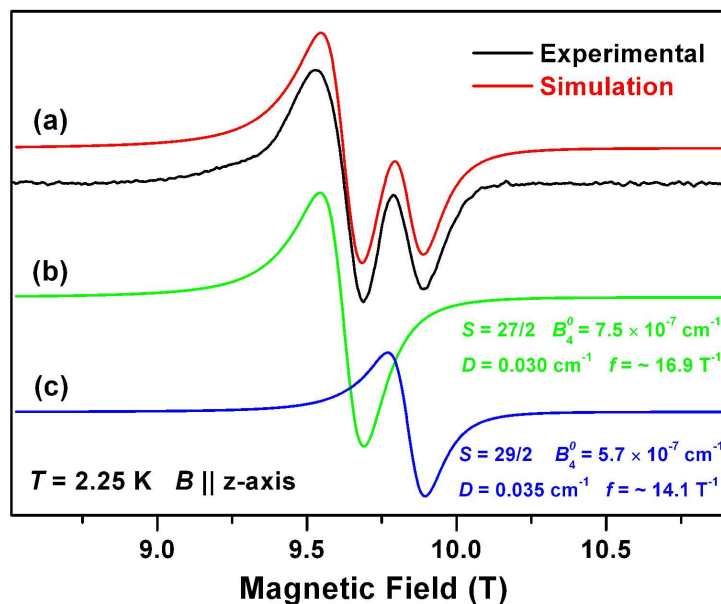


Figure S3. EPR spectrum of a single crystal and its simulation. (a) Black line: the experimental spectrum at 240 GHz and 2.25 K; red line: the simulation under the same conditions, obtained by adding parts (b) and (c). (b) Simulation using $S = 27/2$, $g = 1.996$, $D = 0.030 \text{ cm}^{-1}$, $\Delta D = 0.009(2) \text{ cm}^{-1}$, and $B_4^0 = 7.5(2) \times 10^{-7} \text{ cm}^{-1}$. (c) Simulation using $S = 29/2$, $g = 1.996$, $D = 0.035 \text{ cm}^{-1}$, $\Delta D = 0.007(2) \text{ cm}^{-1}$, and $B_4^0 = 5.7(2) \times 10^{-6} \text{ cm}^{-1}$. The relative EPR intensity ratio of part (b) over part (c) is 2.45.